Stability analysis in an optical lattice clock using the four-path measurement

Xiao-Tong Lu ◉,[1] Feng Guo,[1] Jing-Jing Xia ◉,[1,2] Yan-Yan Liu,[1] Ben-Quan Lu,[1] and Hong Chang ◉[1,2,*]

[1]*National Time Service Center, Chinese Academy of Sciences, Xi'an 710600, China*
[2]*School of Astronomy and Space Science, University of Chinese Academy of Sciences, Beijing 100049, China*

In this paper, we propose a method for identifying the contribution of various sources of noise to the instability of an optical lattice clock. These sources include Dick noise, quantum projection noise, shot noise, and technical noise. By measuring the clock instability at four different sets of parameters, we can determine the frequency fluctuations due to each type of noise separately. Furthermore, we can accurately extract the absolute number of atoms, the photon number detected per atom by the photoelectric detector, and the root mean square fluctuations of the atom number. We demonstrate the effectiveness of our approach through numerical simulations, showcasing the ability to determine these parameters with an uncertainty of less than 10%. Specifically, a remarkable uncertainty of 1% can be achieved when determining the atom number.

I. INTRODUCTION

Optical lattice clocks (OLCs) have achieved remarkable fractional frequency instability of $4.8 \times 10^{-17} \tau^{-0.5}$ (where τ indicates the measurement time shown in seconds), and exceptional measurement precision in the regime of 10^{-21} [1–3]. These advancements have had significant impacts on reducing clock systematic uncertainty [2–6], advancing relativistic geodesy [7,8], generating ultrastable microwave signals [9], and conducting fundamental physics research [10–12].

Clock instability arises from two main sources of noise that contribute to the error signal detected in the clock cycle: Clock laser noise and atomic detection noise [13]. The intermittent interaction of atoms with the clock laser leads to the conversion of high-frequency laser noise to low-frequency noise (referred to as the Dick effect [14,15]), which results in incorrect frequency corrections for the clock laser. The Dick effect can be mitigated by employing zero-dead-time sampling of the clock laser noise using two clocks [16] or through synchronized detection techniques [17–19]. Additionally, nondestructive detection methods [20], improved stability of the clock laser [21–23], and increased duty cycle [14,15] can help reduce the impact of the Dick noise. The atomic detection noise includes quantum projection noise (QPN) [24,25], shot noise from the photoelectric detector, and technical noise arising from dark counts and stray light in the photoelectric detector [13]. The QPN is determined by the atom number and the frequency-sensitive slope of the clock transition spectrum. It can be suppressed by increasing the atom number or overcome utilizing techniques such as squeezed states [26] and atom entanglement [27]. Shot noise and technical noise are associated with the fluorescence detection system and become more significant when the atom number is small [13].

A thorough comprehension of the impact of various noise sources on clock stability is essential for achieving optimal clock performance. Moreover, it enables researchers to determine crucial systematic parameters such as the absolute number of atoms N_0, which is essential for studying many-body interactions [3,28]; the photon count η detected per atom by the photoelectric detector; and the root mean square fluctuations of the atom number δ_N. However, the traditional method to distinguish different noise contributions to stability relies on measuring each noise contribution one by one, which is cumbersome and complicated [13].

This study introduces the four-path measurement (FPM) method, which distinguishes different noise contributions to stability with high precision in optical lattice clocks. Our approach involves conducting four measurements of clock stability under different systematic parameters, rather than based on analysis of the different types of noise from the detection and interrogation laser [13]. By performing numerical simulations, we demonstrate that the FPM method can accurately measure different noise contributions and potentially provide accurate values for N_0, η, and δ_N.

II. THE FOUR-PATH MEASUREMENT METHOD

When considering a transition probability of 0.5 and neglecting the detection laser noise, which can typically be significantly reduced compared to other effects [13], the clock instability σ_{p1} at $\tau = 1$ can be expressed by [17,29]

$$\sigma_{p1}^2 = \sigma_{\text{Dick}}^2 + \sigma_{\text{QPN}}^2 + \sigma_{\text{Shot}}^2 + \sigma_{\text{Det}}^2. \quad (1)$$

In Eq. (1), σ_{Dick}^2 represents the variance of frequency fluctuation caused by the Dick effect. $\sigma_{\text{QPN}}^2 = T_C/4K_0^2 N_0$ corresponds to the variance contributed by the QPN, where T_C is the clock cycle time, and K_0 denotes the absolute value of the frequency-sensitive slope of the spectrum at the half-height points. $\sigma_{\text{Shot}}^2 = T_C/4K_0^2 N_0 \eta$ indicates the variance originating from shot noise, while $\sigma_{\text{Det}}^2 = T_C \delta_N^2/2K_0^2 N_0^2$ represents the contribution of technical noise. Equation (1) is valid only under the precondition that all noises are independent of each other. Since the four terms in Eq. (1) exhibit distinct

*changhong@ntsc.ac.cn

dependencies on N_0 and η, we can utilize experimental measurements to distinguish these noise components effectively. Additionally, we can determine the values of N_0, η, and δ_N by analyzing the measurement results of σ_{QPN}, σ_{Shot}, and σ_{Det}, respectively. The Dick-noise-limited instability can be written as [14]

$$\sigma_{Dick}^2 = \frac{\sigma_{clock}^2}{2ln2} \frac{T_C}{\tau} \sum_{k=1}^{\infty} \frac{1}{k} \left| \frac{g_k}{g_0} \right|^2, \qquad (2)$$

where the frequency flicker noise floor of the clock laser, designated as σ_{clock}, is determined by analyzing the frequency correction signals, with the linear frequency drift removed. Meanwhile, g_k refers to the Fourier coefficients of the frequency-sensitive function. σ_{Dick}^2 exhibits a nonlinear relationship with the duty cycle; however, we can derive σ_{Dick}^2 by altering the clock detection time T_p, the time during which the clock transition is excited by the clock laser, while maintaining T_C constant. When we adjust T_p to $\beta_1 T_p$, the total clock instability can be expressed as

$$\sigma_{p2}^2 = \beta_0 \sigma_{Dick}^2 + \left(\sigma_{QPN}^2 + \sigma_{Shot}^2 + \sigma_{Det}^2 \right) / \beta_1^2. \qquad (3)$$

The precise determination of β_0 can be carried out using Eq. (2). Subsequently, we can determine the other factors associated with atomic detection noises. The value of η is directly proportional to the length of the detection laser pulse (T_{det}), which can be precisely controlled and measured in experiments. By adjusting T_{det} to $\beta_2 T_{det}$ while keeping the other parameters constant as described in Eq. (1), the value of η will become $\beta_2 \eta$. Hence, the total clock instability can be denoted as

$$\sigma_{p3}^2 = \sigma_{Dick}^2 + \sigma_{QPN}^2 + \sigma_{Shot}^2/\beta_2 + \sigma_{Det}^2. \qquad (4)$$

Finally, by changing the atom number from N_0 to $\beta_3 N_0$, we can separate the technical noise from other sources of noise. This modification results in a total clock instability represented by

$$\sigma_{p4}^2 = \sigma_{Dick}^2 + \left(\sigma_{QPN}^2 + \sigma_{Shot}^2 \right)/\beta_3 + \sigma_{Det}^2/\beta_3^2. \qquad (5)$$

Combining Eq. (1) with Eqs. (3)–(5), we have the following equation:

$$\begin{bmatrix} 1 & 1 & 1 & 1 \\ \beta_0 & 1/\beta_1^2 & 1/\beta_1^2 & 1/\beta_1^2 \\ 1 & 1 & 1/\beta_2 & 1 \\ 1 & 1/\beta_3 & 1/\beta_3 & 1/\beta_3^2 \end{bmatrix} \begin{bmatrix} \sigma_{Dick}^2 \\ \sigma_{QPN}^2 \\ \sigma_{Shot}^2 \\ \sigma_{Det}^2 \end{bmatrix} = \begin{bmatrix} \sigma_{T1}^2 \\ \sigma_{T2}^2 \\ \sigma_{T3}^2 \\ \sigma_{T4}^2 \end{bmatrix}. \qquad (6)$$

By solving Eq. (6), we can determine the precise values of σ_{Dick}, σ_{QPN}, σ_{Shot}, and σ_{Det}, thereby inferring the parameters of N_0, η, and δ_N. The measurement of N_0 using the FPM method eliminates the need for precise determination of the solid angle and quantum conversion efficiency of the detection systems, which are typically required in fluorescence detection methods [30]. Additionally, it removes the limitation of having to know the shape of the cold ensemble, which affects the measurement precision of absorption imaging techniques [31]. As a result, the FPM method exhibits great potential for achieving high accuracy. Moreover, the FPM approach allows for the precise measurement of the parameters of η and δ_N, providing an opportunity to validate corresponding measurements obtained through traditional techniques [13].
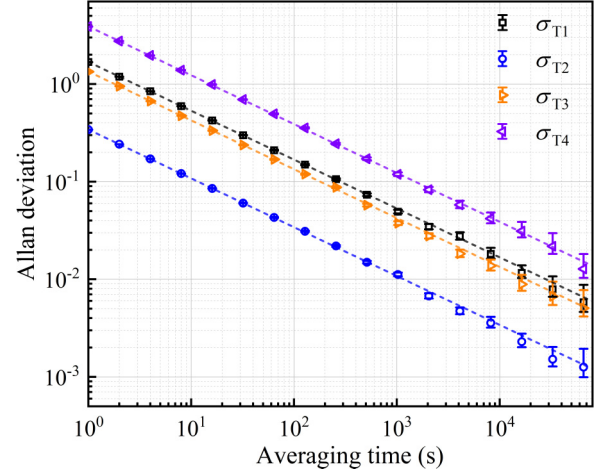

FIG. 1. Frequency stabilities at four-group parameters. The points represent the numerical results, where the single clock stability was inferred by dividing the interleaved self-comparison stability by $\sqrt{2}$. The dotted lines indicate the corresponding theoretical results. Error bars represent the 1σ standard error.

III. NUMERICAL RESULTS

To validate this method, we performed a numerical simulation of the clock operation process [18,32,33] and obtained relevant parameters by analyzing the Allan variance of the self-comparison data. The simulation involved four main steps. In Step 1, we initialized the necessary parameters, including the modulation parameters of β_1–β_3, as well as other systematic parameters such as N_0, η, δ_N, and the drift rate of the clock laser frequency. Additionally, we calculated the Dick limits to determine the value of β_0. Moving on to Step 2, we calculated the standard deviations ($\sigma_{p1} \sim \sigma_{p4}$) and generated noise for the four cases by multiplying normally distributed random numbers by their corresponding standard deviation. Step 3 involved performing the self-comparison operation to measure the stability of the individual clock. In this step, the central frequency of the laser frequency was interleavedly locked to two transitions with independent feedback. By detecting the difference in excitation fractions at the half-width points of the spectrum, the frequency correction can be expressed by $(P_{eR}-P_{eL})/2K_0$, where P_{eR} and P_{eL} are the excitation fractions at the right and left sides of the spectrum, respectively. The noise-induced frequency fluctuations were directly added to the frequency corrections of each interleaved loop. In Step 4, we performed calculations to determine the single clock stabilities. This was done by dividing the self-comparison stability by $\sqrt{2}$ [18]. Once the total stabilities of the four operation cases were determined, we could proceed to derive the contribution of each noise source using Eq. (6). Additionally, we could extract the parameters N_0, η, and δ_N from the analysis results.

Figure 1 shows the Allan deviations (σ_{p1}–σ_{p4}) obtained from both theoretical and numerical results at various parameters, including $\sigma_{clock} = 0.043$ Hz (corresponding to a 10^{-16} instability of strontium optical lattice clocks), $T_p = 0.01$ s, $T_C = 1$ s, $N_0 = 500$, $\eta = 1$, $\delta_N = 3$, $\beta_1 = 5$, $\beta_2 = 3.88$, and $\beta_3 = 0.2$. Here, we choose a small T_p to intentionally increase the contribution of atomic detection noise. The values of η

TABLE I. Comparison of noises amplitudes (represented by the standard deviation) between extracted results using the FPM method and the corresponding theoretical values. The numerical results are derived from a single numerical simulation (shown in Fig. 1), while the uncertainties represent the standard deviation of 50 simulations.

Noise source	Theoretical (Hz)	Extracted (Hz)
σ_{Dick}	0.0778	0.0798(17)
σ_{QPN}	1.1787	1.1691(90)
σ_{Shot}	1.1787	1.1794(17)
σ_{Det}	0.2236	0.2343(200)

and δ_N are from Ref. [17], while $\beta_1 - \beta_3$ are chosen to ensure obvious differences between $\sigma_{p1} - \sigma_{p4}$. Table I presents a comparison between the 1σ frequency fluctuations of different noise sources and their theoretical values. The good agreement between the extracted and theoretical values, within the measurement errors, demonstrates the validity of the FPM method.

We further conducted a numerical study on the measurements of N_0, η, and δ_N using the FPM method. In this study, we varied the setting value of N_0 from 70 to 2050 while keeping σ_{clock} at either 0.43 Hz or 0.043 Hz to investigate the influence of σ_{clock} on the results. The other parameters remained the same as in Fig. 1. Figure 2(a) illustrates the determination of the absolute number of atoms. It can be observed that the uncertainty is larger for smaller values of N_0 due to the presence of strong atomic detection noises, which deteriorate the measurement stability. In the case of $\sigma_{\text{clock}} = 0.43$ Hz, the measurement uncertainty increases with the increase of N_0 as the Dick noise gradually dominates the total noise. However, by reducing σ_{clock} to 0.043 Hz, the atom number can be measured with an uncertainty below 2% over a wide range of N_0.

Figure 2(b) presents the measurements of η, which cannot be accurately obtained using traditional methods so far. With the FPM method, the value of η can be precisely determined within a very wide range of N_0. It is worth noting that in Figs. 2(a) and 2(b), the uncertainties of the group with $\sigma_{\text{clock}} = 0.043$ Hz are insensitive to N_0, whereas in the case of $\sigma_{\text{clock}} = 0.43$ Hz, the uncertainties increase with increasing N_0.

Figure 2(c) depicts the determinations of δ_N for different N_0 values. As N_0 increases, the measurement uncertainty rises more rapidly than the other two parameters. This is because the technical noise is inversely proportional to N_0^2, indicating that an increase in N_0 will rapidly reduce its contribution to the overall uncertainty.

We discovered that the FPM method yielded average values of N_0, η, and δ_N that deviated from their expected values. These deviations resulted in significant inaccuracies when the number of atoms was less than approximately 300. The possible reason for these deviations is that the excitation fraction is not always interrogated precisely at the half-height points of the spectrum. Consequently, determining N_0 and other parameters using a constant maximum slope will lead to incorrect results, as the average slope during actual operation tends to be smaller than the half-height points. When N_0 is
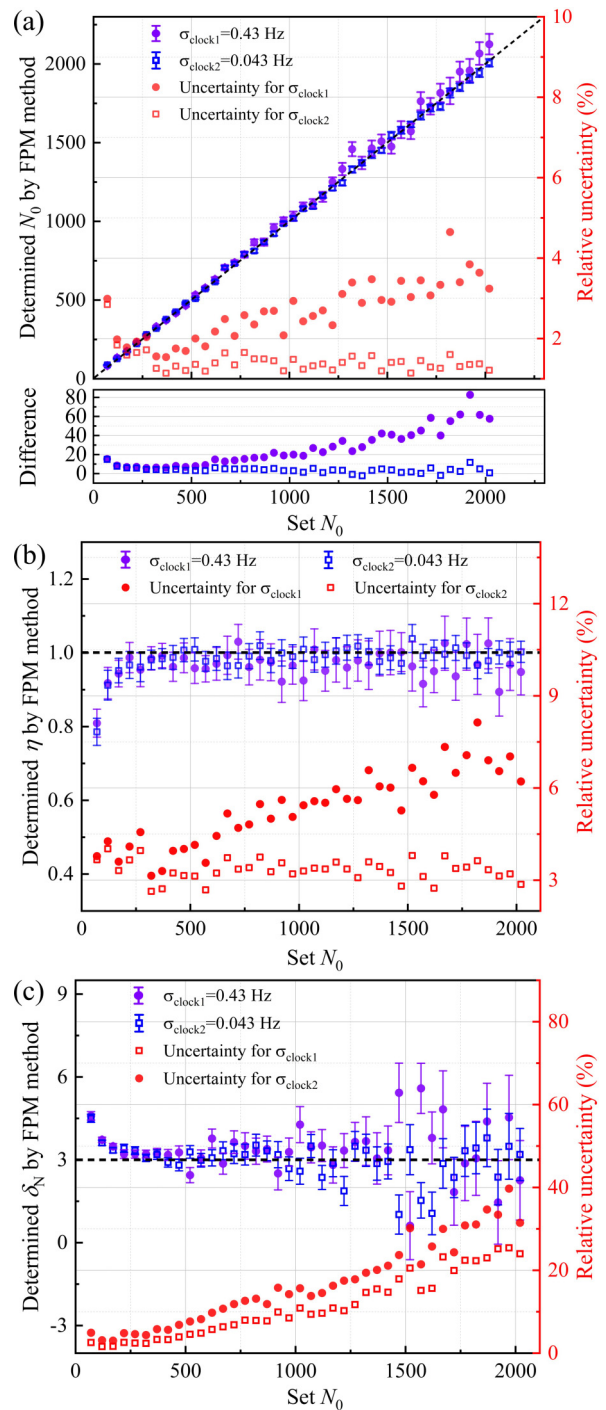

FIG. 2. Numerical results of measurements of the N_0, η, and δ_N. (a) Top: The absolute number of atoms N_0 as a function of the setting atom number. The dashed line indicates the theoretical values. Bottom: The difference between the numerical and theoretical results. (b) The inferred value of η (the theoretical value of 1 represented by the dashed line) at different setting N_0. (c) The extracted value of δ_N at different setting N_0. The dashed line shows the theoretical value of 3. All error bars represent the standard deviation of 50 independent simulations. The simulation results using $\sigma_{\text{clock1}} = 0.43$ Hz are indicated by dots, while squares represent the results using $\sigma_{\text{clock2}} = 0.043$ Hz. The uncertainties in [(a)–(c)] are obtained by dividing the error bars by the corresponding theoretical value.
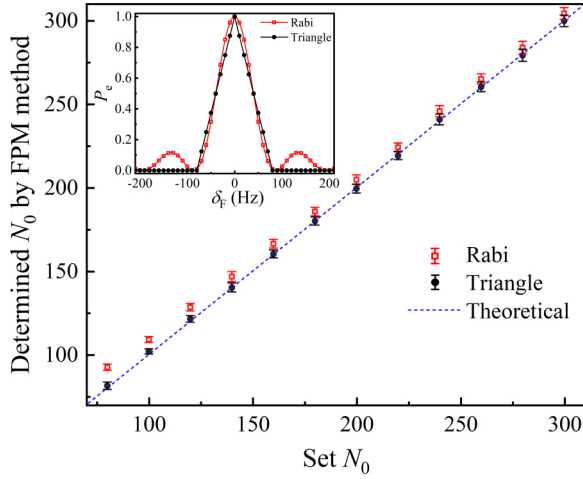
FIG. 3. Measurements of N_0 by the FPM method based on the Rabi and triangular spectra. The inset depicts the Rabi and triangular spectra utilized in this study, wherein δ_F denotes frequency detuning and P_e represents excitation fraction. Error bars indicate the standard deviation of 50 independent simulations.

lower, there is a stronger fluctuation in the excitation fraction, leading to larger deviations. This phenomenon may also explain why larger clock laser noise corresponds to a larger offset, as shown in Fig. 2. To validate the aforementioned hypothesis, we conducted a comparison of N_0 measurement results using the FPM method with both Rabi and triangular spectra. These measurements were performed under identical linewidth and other parameters ($\sigma_{clock} = 0.43$ Hz). The triangular spectrum, characterized by a consistent frequency-sensitivity slope, remains unaffected by fluctuations in the excitation fraction. In Fig. 3, we present the numerical results which validate our inference. It is worth noting that while achieving the triangular spectrum is challenging, this phenomenon suggests that the FPM method can effectively function with $\sigma_{clock} = 0.43$ Hz when N_0 exceeds 300.

Under the same modulation parameters, it is impossible to simultaneously determine the values of N_0, η, and δ_N with the smallest uncertainty, highlighting the need to optimize the values of β_1–β_3 for accurate measurements of the target. To investigate the relationship between the measurement uncertainties of N_0, η, and δ_N with β_1, β_2, and β_3, respectively, we conducted numerical research as shown in Figs. 4(a)–4(c). In this study, we specified the following values: $N_0 = 500$, $\sigma_{clock} = 0.043$ Hz, $T_p = 0.01$ s, $T_C = 1$ s, $\eta = 1$, and $\delta_N = 3$. Moreover, we adjusted the values of β_1–β_3 from 0.1 to approximately 8, a parameter range that is experimentally attainable in OLCs [2,18]. When β_1, β_2, and β_3 approach 1, all measurements fail due to a near-zero measurement lever arm. Within the calculated parameter region, the smallest measurement uncertainties for N_0, η, and δ_N are 1% ($\beta_1 = 5$, $\beta_2 = 3.88$, and $\beta_3 = 0.2$), 2.3% ($\beta_1 = 5$, $\beta_2 = 7.24$, and $\beta_3 = 0.2$), and 6.3% ($\beta_1 = 5$, $\beta_2 = 1.99$, and $\beta_3 = 0.2$), respectively. It is possible to achieve even lower measurement uncertainty if a larger parameter region is considered.
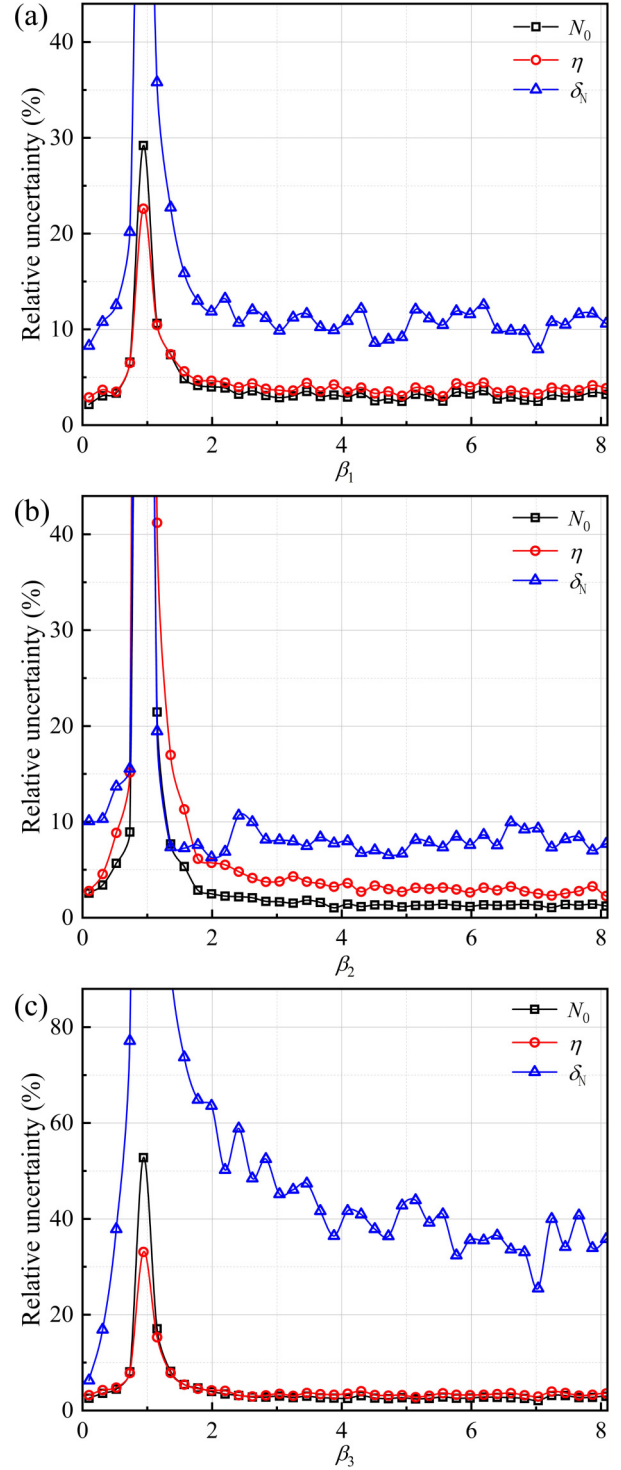

FIG. 4. Effects of modulation parameters on the measurement uncertainties of N_0, η, and δ_N. (a) Measurement uncertainties as a function of β_1, keeping the values of $\beta_2 = 3.88$ and $\beta_3 = 0.2$. (b) Dependence of measurement uncertainties on the choice of β_2, with $\beta_1 = 5$ and $\beta_3 = 0.2$. (c) The case of changing β_3 while maintaining constant values of $\beta_1 = 5$ and $\beta_2 = 3.88$. For all figures, squares, circles, and triangles indicate standard deviation of 50 independent simulations of N_0, η, and δ_N, respectively.
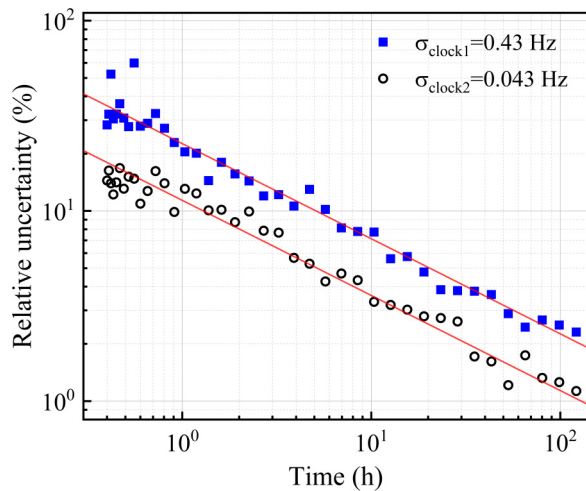
FIG. 5. Relative uncertainty of the atom number measurement using the FPM method as a function of time consumption. The relative uncertainty is obtained by dividing the standard deviation of 50 numerical simulations by the atom number set at 1000. The red solid lines indicate the linear fitting with a fixed slope of -0.5.

Studying the relationship between total time consumption and measurement uncertainty using the FPM method is also an interesting avenue to explore, as they are critical in experiments. Figure 5 depicts the relative uncertainty as a function of the total measurement time. The uncertainties decrease with increasing time at a slope of -0.5, which coincides with the fact that the clock-comparison instability decreases with averaging time at the same slope of -0.5. Based on linear regression, achieving a 10% uncertainty (the typical uncertainty of the absorption imaging method [30,31]) requires a measurement time of 5 (or 1.3) h for $\sigma_{\mathrm{clock}} = 0.43$ (or 0.043) Hz.

IV. CONCLUSION

We have developed a four-path measurement method to distinguish the contribution of Dick noise, QPN noise, shot noise, and technical noise on stability in an optical lattice clock. This method enables us to determine the systematic parameters of N_0, η, and δ_{N} with high accuracy by separating these noise contributions. Through numerical simulations, we demonstrate that our method can achieve a measurement uncertainty of 1% for N_0, 2.3% for η, and 6.3% for δ_{N}. The measurement precision of N_0 demonstrated in this work is superior to that of the absorption imaging method [30,31], which typically has a measurement uncertainty of 10% limited by the knowledge of cold-ensemble shape and technical noises, and cannot be improved by increasing measurement time. This work not only enhances our understanding of the system in noise contribution but also has the potential to facilitate other research areas such as many-body interaction [3,28], nondestructive detection [20], and entanglement of atoms [27] that benefit from the high precision of atom number measurement. This method can be easily extended to other systems, such as atomic fountain clocks [29,34].

[1] E. Oelker, R. B. Hutson, C. J. Kennedy, L. Sonderhouse, T. Bothwell, A. Goban, D. Kedar, C. Sanner, J. M. Robinson, G. E. Marti, D. G. Matei, T. Legero, M. Giunta, R. Holzwarth, F. Riehle, U. Sterr, and J. Ye, Nat. Photon. **13**, 714 (2019).

[2] T. Bothwell, C. J. Kennedy, A. Aeppli, D. Kedar, J. M. Robinson, E. Oelker, A. Staron, and J. Ye, Nature (London) **602**, 420 (2022).

[3] A. Aeppli, A. Chu, T. Bothwell, C. J. Kennedy, D. Kedar, P. He, A. M. Rey, and J. Ye, Sci. Adv. **8**, eadc9242 (2022).

[4] T. Bothwell, D. Kedar, E. Oelker, J. M. Robinson, S. L. Bromley, W. L. Tew, J. Ye, and C. J. Kennedy, Metrologia **56**, 065004 (2019).

[5] K. Kim, A. Aeppli, T. Bothwell, and J. Ye, Phys. Rev. Lett. **130**, 113203 (2023).

[6] R. Schwarz, S. Dörscher, A. Al-Masoudi, E. Benkler, T. Legero, U. Sterr, S. Weyers, J. Rahm, B. Lipphardt, and C. Lisdat, Phys. Rev. Res. **2**, 033242 (2020).

[7] W. F. McGrew, X. Zhang, R. J. Fasano, S. A. Schäffer, K. Beloy, D. Nicolodi, R. C. Brown, N. Hinkley, G. Milani, M. Schioppo, T. H. Yoon, and A. D. Ludlow, Nature (London) **564**, 87 (2018).

[8] J. Grotti, S. Koller, S. Vogt, S. Hfner, U. Sterr, C. Lisdat, H. Denker, C. Voigt, L. Timmen, A. Rolland *et al.*, Nat. Phys. **14**, 437 (2018).

[9] T. Nakamura, J. Davila-Rodriguez, H. Leopardi, J. A. Sherman, T. M. Fortier, X. Xie, J. C. Campbell, W. F. McGrew, X. Zhang, Y. S. Hassan, D. Nicoldi *et al.*, Science **368**, 889 (2020).

[10] M. Filzinger, S. Dörscher, R. Lange, J. Klose, M. Steinel, E. Benkler, E. Peik, C. Lisdat, and N. Huntemann, Phys. Rev. Lett. **130**, 253001 (2023).

[11] M. Takamoto, I. Ushijima, N. Ohmae, T. Yahagi, K. Kokado, H. Shinkai, and H. Katori, Nat. Photon. **14**, 411 (2020).

[12] H. Miyake, N. C. Pisenti, P. K. Elgee, A. Sitaram, and G. K. Campbell, Phys. Rev. Res. **1**, 033113 (2019).

[13] A. Al-Masoudi, S. Dörscher, S. Häfner, U. Sterr, and C. Lisdat, Phys. Rev. A **92**, 063814 (2015).

[14] G. J. Dick, in *Proceedings of the 19th Annual Precise Time and Time Interval Meeting, Redendo Beach, 1987* (US Naval Observatory, Washington, DC, 1988), pp. 133–147.

[15] P. G. Westergaard, J. Lodewyck, and P. Lemonde, IEEE Trans. Ultrason., Ferroelect., Freq. Contr. **57**, 623 (2010).

[16] M. Schioppo, R. C. Brown, W. F. McGrew, N. Hinkley, R. J. Fasano, K. Beloy, T. H. Yoon, G. Milani, D. Nicolodi, J. A. Sherman, N. B. Phillips, C. W. Oates, and A. D. Ludlow, Nat. Photon. **11**, 48 (2017).

[17] M. Takamoto, T. Takano, and H. Katori, Nat. Photon. **5**, 288 (2011).

[18] T. L. Nicholson, M. J. Martin, J. R. Williams, B. J. Bloom, M. Bishof, M. D. Swallows, S. L. Campbell, and J. Ye, Phys. Rev. Lett. **109**, 230801 (2012).

[19] X. T. Lu, C. H. Zhou, T. Li, Y. B. Wang, and H. Chang, Appl. Phys. Lett. **117**, 231101 (2020).

[20] D. B. Orenes, R. J. Sewell, J. Lodewyck, and M. W. Mitchell, Phys. Rev. Lett. **128**, 153201 (2022).

[21] D. G. Matei, T. Legero, S. Häfner, C. Grebing, R. Weyrich, W. Zhang, L. Sonderhouse, J. M. Robinson, J. Ye, F. Riehle, and U. Sterr, Phys. Rev. Lett. **118**, 263202 (2017).

[22] W. Zhang, J. M. Robinson, L. Sonderhouse, E. Oelker, C. Benko, J. L. Hall, T. Legero, D. G. Matei, F. Riehle, U. Sterr, and J. Ye, Phys. Rev. Lett. **119**, 243601 (2017).

[23] J. L. Yu, S. Häfner, T. Legero, S. Herbers, D. Nicolodi, C. Y. Ma, F. Riehle, and U. Sterr, Phys. Rev. X **13**, 041002 (2023).

[24] W. M. Itano, J. C. Bergquist, J. J. Bollinger, J. M. Gilligan, D. J. Heinzen, F. L. Moore, M. G. Raizen, and D. J. Wineland, Phys. Rev. A **47**, 3554 (1993); **51**, 1717(E) (1995).

[25] G. Santarelli, Ph. Laurent, P. Lemonde, A. Clairon, A. G. Mann, S. Chang, A. N. Luiten, and C. Salomon, Phys. Rev. Lett. **82**, 4619 (1999).

[26] W. J. Eckner, N. D. Oppong, A. Cao, A. W. Young, W. R. Milner, J. M. Robinson, J. Ye, and A. M. Kaufman, Nature (London) **621**, 734 (2023).

[27] E. Pedrozo-Peñafie, S. Colombo, C. Shu, A. F. Adiyatullin, Z. Y. Li, E. Mendez, B. Braverman, A. Kawasaki, D. Akamatsu, Y. H. Xiao, and V. Vuletić, Nature (London) **588**, 414 (2020).

[28] A. M. Rey, A. V. Gorshkov, C. V. Kraus, M. J. Martin, M. Bishof, M. D. Swallows, X. Zhang, C. Benko, J. Ye, N. D. Lemke, and A. D. Ludlow, Ann. Phys. **340**, 311 (2014).

[29] H. Zhang, J. Ruan, D. D. Liu, F. Yang, S. C. Fan, Y. Bai, Y. Guan, X. L. Wang, J. R. Shi, and S. G. Zhang, IEEE Trans. Instrum. Meas. **71**, 1008312 (2022).

[30] O. K. Gregor, P. Melina, W. Gustav, C. C. Paul, S. Daniel, B. Mark, M. Olivier, and K. Wolf von, Cent. Eur. J. Phys. **10**, 1054 (2012).

[31] G. Reinaudi, T. Lahaye, Z. Wang, and D. Guery-Odelin, Opt. Lett. **32**, 3143 (2007).

[32] X. T. Lu, M. J. Yin, T. Li, Y. B. Wang, and H. Chang, Jpn. J. Appl. Phys. **59**, 070903 (2020).

[33] C. H. Zhou, X. T. Lu, B. Q. Lu, Y. B. Wang, and H. Chang, Appl. Sci. **11**, 1206 (2021).

[34] T. P. Heavner, E. A. Donley, F. Levi, G. Costanzo, T. E. Parker, J. H Shirley, N. Ashby, S. Barlow, and S. R. Jefferts, Metrologia **51**, 174 (2014).

Correction: The previously published Figure 3 was missing the inset and has been replaced.